LETTER

doi:10.1038/nature10180

Subunit arrangement and phenylethanolamine binding in GluN1/GluN2B NMDA receptors

Erkan Karakas[1], Noriko Simorowski[1] & Hiro Furukawa[1]

Since it was discovered that the anti-hypertensive agent ifenprodil has neuroprotective activity through its effects on NMDA (*N*-methyl-D-aspartate) receptors[1], a determined effort has been made to understand the mechanism of action and to develop improved therapeutic compounds on the basis of this knowledge[2–4]. Neurotransmission mediated by NMDA receptors is essential for basic brain development and function[5]. These receptors form heteromeric ion channels and become activated after concurrent binding of glycine and glutamate to the GluN1 and GluN2 subunits, respectively. A functional hallmark of NMDA receptors is that their ion-channel activity is allosterically regulated by binding of small compounds to the amino-terminal domain (ATD) in a subtype-specific manner. Ifenprodil and related phenylethanolamine compounds, which specifically inhibit GluN1 and GluN2B NMDA receptors[6,7], have been intensely studied for their potential use in the treatment of various neurological disorders and diseases, including depression, Alzheimer's disease and Parkinson's disease[2,4]. Despite considerable enthusiasm, mechanisms underlying the recognition of phenylethanolamines and ATD-mediated allosteric inhibition remain limited owing to a lack of structural information. Here we report that the GluN1 and GluN2B ATDs form a heterodimer and that phenylethanolamine binds at the interface between GluN1 and GluN2B, rather than within the GluN2B cleft. The crystal structure of the heterodimer formed between the GluN1b ATD from *Xenopus laevis* and the GluN2B ATD from *Rattus norvegicus* shows a highly distinct pattern of subunit arrangement that is different from the arrangements observed in homodimeric non-NMDA receptors and reveals the molecular determinants for phenylethanolamine binding. Restriction of domain movement in the bi-lobed structure of the GluN2B ATD, by engineering of an inter-subunit disulphide bond, markedly decreases sensitivity to ifenprodil, indicating that conformational freedom in the GluN2B ATD is essential for ifenprodil-mediated allosteric inhibition of NMDA receptors. These findings pave the way for improving the design of subtype-specific compounds with therapeutic value for neurological disorders and diseases.

The consensus view that has emerged from functional studies of NMDA receptors using site-directed mutagenesis and molecular modelling is that phenylethanolamine compounds such as ifenprodil and Ro 25-6981 bind to the ATD of the GluN2B subunit. However, this has not been established directly and the mechanism of action is complicated by the obligate heteromeric assembly of NMDA receptors. To establish directly that phenylethanolamines bind to the ATDs of these receptors, we used isothermal titration calorimetry to measure the binding of ifenprodil and Ro 25-6981 to purified recombinant *Rattus norvegicus* GluN2B (residues 31–394) and *Xenopus laevis* GluN1b (residues 23–408) ATDs (Supplementary Fig. 1). GluN1b from *Xenopus laevis*[8,9] was used in this study because of its superior biochemical stability compared to other orthologues. It is 93% identical in primary sequence to the *Rattus norvegicus* GluN1 ATD and is capable of forming functional NMDA-receptor ion channels that undergo ifenprodil inhibition when combined with *Rattus norvegicus* GluN2B[9] (Supplementary Fig. 2). When the GluN1b ATD or GluN2B ATD proteins were individually injected with ifenprodil, there was no evidence of binding (Fig. 1a). However, when a mixture of the GluN1b and GluN2B ATD proteins was injected with ifenprodil or Ro 25-6981, a dose-dependent heat exchange was observed, with dissociation constant (K_d) values of 320 nM and 60 nM, respectively (Fig. 1a and Supplementary Fig. 3). Thus, both the GluN1b and GluN2B ATDs are required for binding of phenylethanolamines.

The necessity of both ATDs for recognition of phenylethanolamine indicates that binding takes place in the GluN1–GluN2B heteromer. To probe the association pattern of GluN1b and GluN2B ATD proteins,

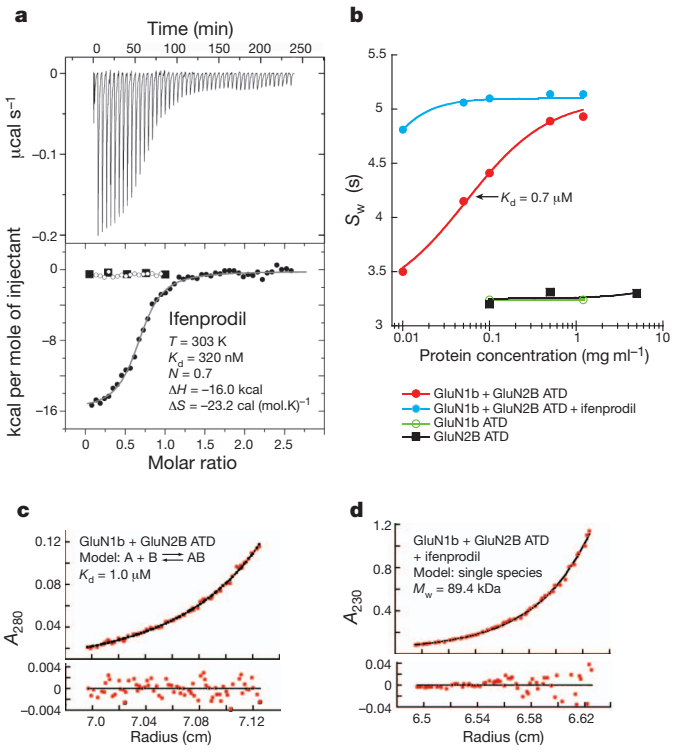

Figure 1 | Binding of phenylethanolamine requires both GluN1b and GluN2B ATDs, and stabilizes heterodimers. **a**, Calorimetric titration of ifenprodil into a GluN1b and GluN2B ATD mixture (upper panel) and integrated heat as a function of the ifenprodil/protein molar ratio (lower panel) for GluN1b ATD (open circles), GluN2B ATD (filled squares) and the GluN1b/GluN2B ATD mixture (filled circles). **b**, Weighted-average sedimentation coefficient (S_w) for GluN1b ATD alone (green), GluN2B ATD alone (black) and the GluN1b–GluN2B ATD mixture in the presence (cyan) and absence (red) of 10 μM ifenprodil, fitted with a monomer-dimer model (lines). **c**, **d**, Sedimentation equilibrium analysis of GluN1b and GluN2B ATDs in the absence (**c**) and presence (**d**) of 10 μM ifenprodil. Data points at a rotor speed of 18,000 r.p.m. (red dots) are shown with a global fit (black line) of the data. Residuals from the fit are shown in the lower panel.

[1]Cold Spring Harbor Laboratory, WM Keck Structural Biology Laboratory, 1 Bungtown Road, Cold Spring Harbor, New York 11724, USA.

we determined the mass of the ATD proteins in solution by sedimentation experiments (Fig. 1b–d). Although the individual GluN1b ATD and GluN2B ATD were exclusively monomeric at 1.2 mg ml^{-1} (Fig. 1b), they formed a heterodimer with a K_d of 0.7–1 μM when mixed together (Fig. 1b, c). Notably, when ifenprodil was included in the GluN1b/GluN2B ATD protein mixture, the heterodimerization was strengthened by at least 20-fold (Fig. 1b, d). These results establish that the GluN1b and GluN2B ATDs form heterodimers and that phenylethanolamines probably bind at the GluN1b–GluN2B subunit interface.

To understand the nature of the subunit interaction between GluN1b and GluN2B at their ATDs, and to pinpoint the location of the phenylethanolamine binding site, we conducted crystallographic studies on the GluN1b and GluN2B ATD proteins (Supplementary Table 1). The crystallographic analysis showed that the GluN1b and GluN2B ATDs exist as heterodimers in both ifenprodil-bound and Ro 25-6981-bound forms (Fig. 2). No notable structural difference was observed between the monomers of GluN1b ATD (Supplementary Fig. 4) or GluN2B ATD[10] and the respective subunits in the GluN1b–GluN2B ATD complex, indicating that dimerization did not cause changes in the overall conformation. Most notably, the crystal structures clearly identified the phenylethanolamine binding site at the heterodimer interface (Fig. 2).

Both the GluN1b and GluN2B ATDs have bi-lobed clamshell-like architectures composed of R1 and R2 domains that are roughly similar in secondary-structure distribution to non-NMDA-receptor ATDs[11–14]. However, the structures of the GluN1b and GluN2B ATD monomers cannot be superimposed onto non-NMDA-receptor ATD monomers, owing to a major difference in the R1–R2 orientations, as was also observed previously in a study of the GluN2B ATD monomer[10] (Supplementary Fig. 5). The unique R1–R2 orientations of the GluN1 and GluN2B ATDs result in a heterodimer assembly that is distinct from that observed in non-NMDA-receptor ATD homodimers[11–14] (Supplementary Fig. 6). Whereas non-NMDA-receptor ATD subunits form symmetrical homodimers through strong R1–R1 and R2–R2 interactions, the GluN1b and GluN2B ATDs associate with each other asymmetrically through R1–R1 and R1(GluN1b)–R2(GluN2B) interactions[11,12] (Fig. 2). No residue from GluN1b R2 is involved in the GluN1b–GluN2B interaction (Fig. 2b). The R1–R1 interface contains hydrophobic interactions mediated by residues from the cores of the α2 helix and α3 helix in GluN1b, and from the α1′ helix and α2′ helix in GluN2B, surrounded by polar interactions involving the GluN1b α2 helix, the GluN2B α1′ helix and the hypervariable loops[10] (Supplementary Fig. 7). The R1–R2 interface involves mainly polar interactions, involving residues on the α10 helix, a loop extending from η2 in GluN1b and loops extending from the β6′ sheet and β7′ sheet in GluN2B (Fig. 2d). The lack of R2–R2 interaction in the GluN1b and GluN2B ATDs leaves sufficient room for the previously suggested conformational movement of the bi-lobed structure in GluN2B[10,15], which is important in mediating the allosteric regulation that is unique to NMDA receptors. In non-NMDA receptors, such movement is prohibited, owing to strong R2–R2 interactions that lock the movement of R2 (refs 3, 11–13).

The heterodimeric arrangement of GluN1b and GluN2B creates a phenylethanolamine binding pocket composed of residues from GluN1b R1, GluN2B R1 and GluN2B R2 (Fig. 2). The phenylethanolamine binding site has no overlap with the zinc binding site that is located in the GluN2B ATD cleft[10,16] (Supplementary Fig. 8). In the crystal structure, ifenprodil is buried in the dimer interface with insufficient space for entering or exiting (Fig. 2b), which indicates that binding occurs through an induced-fit mechanism and that unbinding may involve opening of the GluN2B ATD bi-lobed structure. All of the residues at the binding sites are identical among *Xenopus laevis*, rat and human orthologues, indicating that inhibition of NMDA receptors by phenylethanolamine is a conserved feature among those species (Supplementary Fig. 9). Binding of both ifenprodil and Ro 25-6981 is

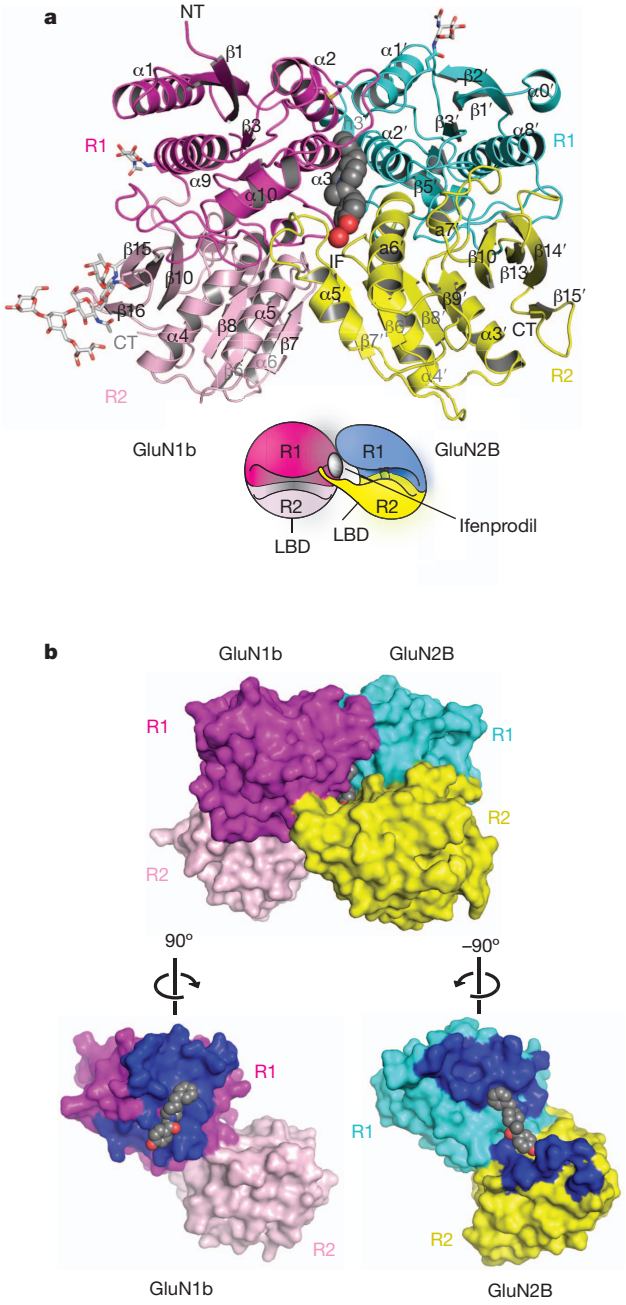

Figure 2 | Structure of the GluN1b–GluN2B ATD heterodimer in complex with ifenprodil at 2.6 Å resolution. **a**, View of the ATD heterodimer from the side. The GluN1b and GluN2B ATDs have bi-lobed architecture composed of R1 (magenta and cyan) and R2 (light pink and yellow) domains. Ifenprodil (grey spheres) sits at the heterodimer interface. *N*-glycosylation chains are shown in white. NT, N terminus; CT, C terminus. The cartoon shows an approximate orientation of the GluN1b and GluN2B ATDs with black sticks below R2 indicating the C-terminal ends where ligand-binding domains (LBDs) begin. **b**, Surface presentation of the GluN1b–GluN2B ATD heterodimer (upper panel) and of each subunit (lower panel), showing residues at the subunit interface in dark blue. Note that ifenprodil (grey spheres) is occluded in the subunit interface. The heterodimer buries 1,191 Å^2 of solvent-accessible surface area per subunit, with the GluN1b R1–GluN2B R1 and GluN1b R1–GluN2B R2 interfaces contributing 62% and 38%, respectively.

mediated primarily through hydrophobic interactions between the benzylpiperidine group and a cluster of hydrophobic residues from the GluN1b α2 helix and α3 helix and the GluN2B α1′ helix and α2′ helix, and between the hydroxylphenyl groups and GluN1b Leu 135, GluN2B Phe 176 and GluN2B Pro 177 (Fig. 3a, b). Furthermore, the

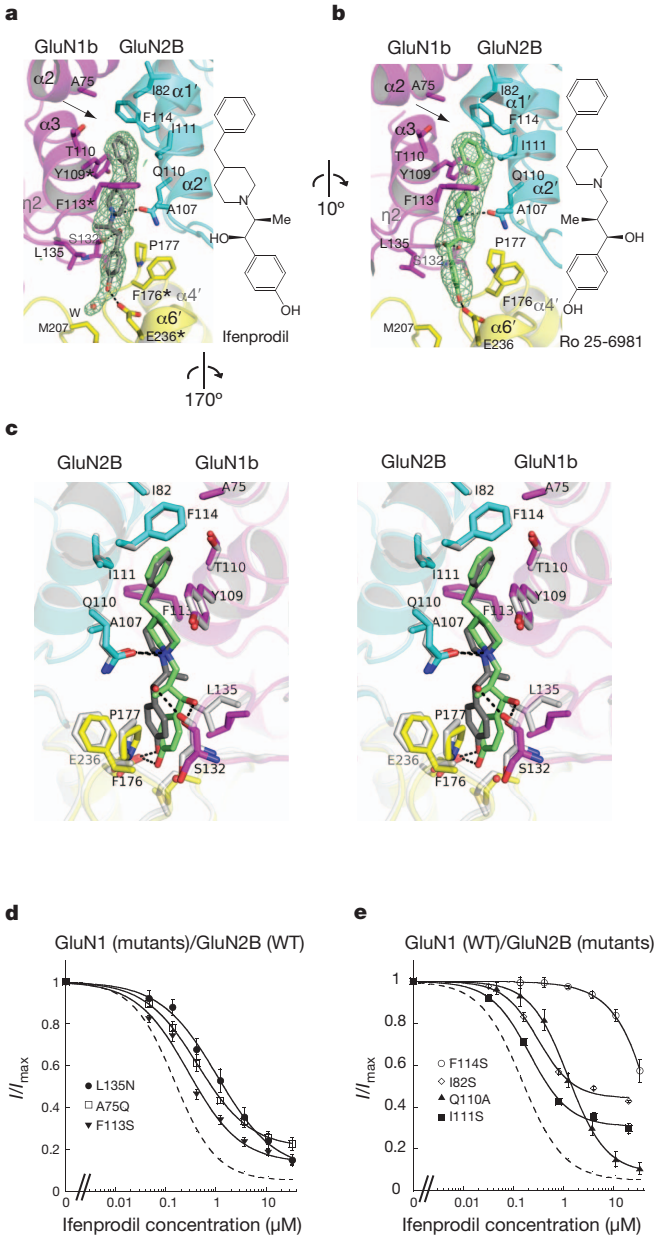

Figure 3 | Phenylethanolamine binding site. **a**, **b**, Binding of ifenprodil (**a**) and Ro 25-6981 (**b**) takes place at the GluN1b–GluN2B subunit interface. Mesh represents the F_o-F_c omit electron density map contoured at 3σ. Residues marked with asterisks in **a** have been previously shown to affect ifenprodil sensitivity. Adjacent to the binding pocket is an empty space surrounded by hydrophobic residues, including GluN1b Ala 75, GluN2B Ile 82 and GluN2B Phe 114 (arrows). **c**, Comparison of binding patterns of ifenprodil (grey) and Ro 25-6981 (lime) in stereoview. The structure bound to Ro 25-6981 is coloured as in **b**, whereas the ifenprodil-bound structure is coloured white. **d**, **e**, New residues found to interact with phenylethanolamines in this study were mutated and analysed for their effect on sensitivity to ifenprodil. Mutation of the residues surrounding the binding site caused changes in IC_{50} as well as changes in the extent of inhibition by ifenprodil. WT, wild-type; I/I_{max}, relative current with (I) and without (I_{max}) ifenprodil. Error bars represent s.d.

drugs make three direct polar interactions with Ser 132 of GluN1b, Gln 110 of GluN2B and Asp 236 of GluN2B. Superposition of the binding sites of ifenprodil and Ro 25-6981 shows that the methyl and hydroxyl groups in the propanol moiety of both ligands face in opposite directions and that the benzylpiperidine groups sit in the binding pocket in similar ways (Fig. 3c). Consequently, Ro 25-6981 has a higher affinity for GluN1/GluN2B NMDA receptors than ifenprodil[17] because the methyl group in Ro 25-6981 is in a favourable position to form a hydrophobic interaction involving Phe 176 and Pro 177 in the GluN2B subunit, whereas ifenprodil makes a weaker hydrophobic interaction with GluN1b, involving Leu 135. Extensive mutagenesis studies have previously indicated that GluN1b Tyr 109 (ref. 18) and GluN2B Phe 176 and Asp 236 (ref. 19) are critical in mediating inhibition by ifenprodil, but whether these are involved in binding or transducing the inhibitory effect was unknown. We performed additional mutagenesis studies on newly identified residues in both GluN1b and GluN2B at the ifenprodil binding site, measured macroscopic currents by two-electrode voltage clamp, and revealed significant alterations in IC_{50} and in the extent of inhibition (Fig. 3d, e and Supplementary Table 2), thereby confirming the physiological relevance of the binding site. Notably, disruption of the 'empty' hydrophobic space formed by GluN1b Ala 75, GluN2B Ile 82 and GluN2B Phe 114 (arrows in Fig. 3a and b) by site-directed mutations to hydrophilic residues had marked effects on sensitivity to ifenprofil (Fig. 3d, e). Thus, stabilization of this hydrophobic space by filling it with a hydrophobic moiety may be a valid strategy to improve the design of phenylethanolamine-based drugs.

It is not known why phenylethanolamine binds specifically to the GluN1–GluN2B subunit combination. Although inspection of the primary sequences shows non-conservation of the critical binding-site residues between GluN2B and GluN2C or GluN2D (for example, the equivalent residue to GluN2B Phe 176 is not conserved in GluN2C or GluN2D), all of the residues in GluN2A are conserved except for GluN2B Ile 111 (Met 112 in GluN2A) (Supplementary Fig. 10). Indeed, the mutations GluN2A Met112Ile or GluN2B Ile111Met do not confer or abolish ifenprodil sensitivity in GluN1/GluN2A or GluN1/GluN2B receptors, respectively (Supplementary Table 2). Thus, the insensitivity of the GluN1/GluN2A receptors to phenylethanolamine may stem from a fundamental difference in the mode of subunit association between GluN1/GluN2A and GluN1/GluN2B at their ATDs.

To validate further the physiological relevance of the heterodimeric assembly, we engineered cysteine mutants at the subunit interface, using the ifenprodil-bound GluN1b/GluN2B ATD structure as a guide, in the context of the intact rat GluN1-4b/GluN2B receptor. These cysteines were designed to form spontaneous disulphide bonds if the mutated residues were proximal to each other. We designed two pairs of cysteine mutants, GluN1-4b (Asn70Cys) with GluN2B (Thr324Cys), and GluN1-4b (Leu341Cys) with GluN2B (Asp210Cys). These mutations 'lock' the R1–R1 and R1–R2 interfaces, respectively (Fig. 4a). We then expressed the mutant receptors in mammalian cell cultures and analysed them for formation of disulphide-linked oligomers in western blots. When mutant receptors of one subunit were co-expressed with wild-type receptors of the other, they gave rise to monomeric bands that were identical to wild-type GluN1-4b–GluN2B receptors in both reducing and non-reducing conditions (110 kDa and 170 kDa for GluN1-4b and GluN2B, respectively; Fig. 4b, arrows 2 and 3). In contrast, co-expressing pairs of the GluN1-4b–GluN2B cysteine mutants gave rise to a heterodimeric ~280 kDa band that was recognized by both anti-GluN1 and anti-GluN2B antibodies in non-reducing conditions (Fig. 4b, arrow 1). This confirms that the R1–R1 and R1–R2 subunit interfaces observed in the GluN1b–GluN2B ATD crystal structures are physiological and that the heterodimer, not the homodimer, is the basic functional unit in the ATD of the NMDA receptor[20]. Furthermore, disulphide crosslinking was observed in the presence and absence of ifenprodil, indicating that the ligand-free GluN1b–GluN2B ATDs may oscillate between the previously suggested open conformation[15] and the closed conformation represented by the crystal structure described here.

To understand the functional effects of locking the R1–R1 and R1–R2 interactions in the GluN1b and GluN2B ATDs, we measured macroscopic current responses from the ion channels of the cysteine-mutant receptors by two-electrode voltage clamp. First, we explored the effect on ion-channel activity of breaking the disulphide bonds.

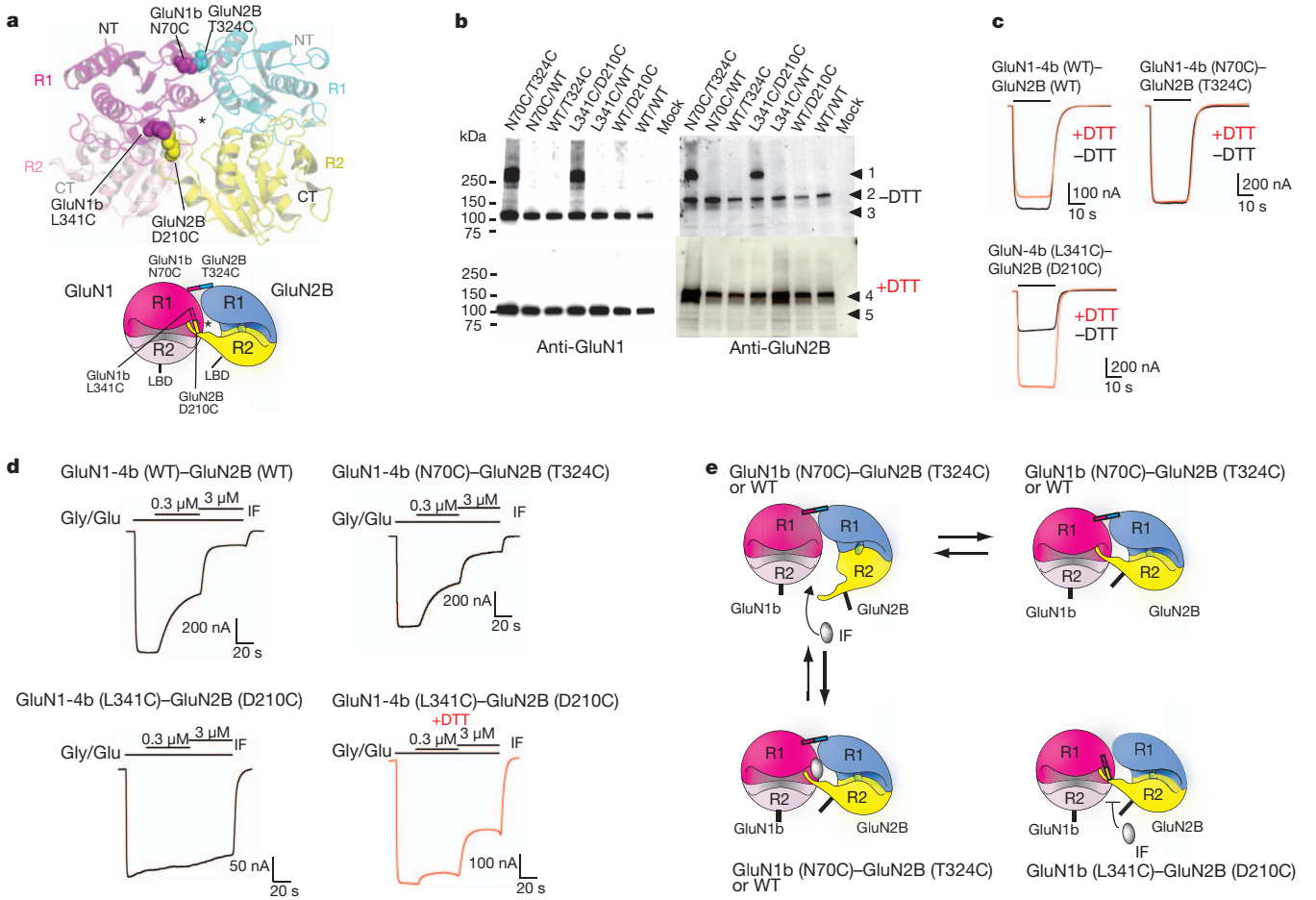

Figure 4 | Engineering of disulphide bonds at the subunit interface alters sensitivity to ifenprodil. a, Location of mutated residues at the R1–R1 and R1–R2 interfaces in the GluN1b and GluN2B ATDs (spheres), and location of the ifenprodil binding pocket (asterisk). **b**, Detection of disulphide bonds by anti-GluN1 and anti-GluN2B western blots in reducing (+DTT) and non-reducing (−DTT) conditions. Arrow 1, GluN1-4b–GluN2B heterodimer; arrows 2 and 4, GluN2B monomers; arrows 3 and 5, GluN1-4b monomers. **c**, Macroscopic current recording of the wild-type and mutant receptors in the presence (red) and absence (black) of DTT (2 mM). **d**, Effect of disulphide bonds on the sensitivity to ifenprodil (IF) of wild-type and mutant receptors in the presence (red) and absence (black) of DTT. **e**, Possible model of ifenprodil binding and the movement of ATDs for allosteric inhibition. Ifenprodil binds to the open GluN2B clamshell and induces domain closure, resulting in allosteric inhibition. In the GluN1-4b (Asn70Cys)–GluN2B (Thr324Cys) receptor, the GluN2B ATD is locked in the closed conformation so ifenprodil cannot access the binding site.

Application of dithiothreitol (DTT) had a minor inhibitory effect on wild-type GluN1-4b–GluN2B receptors and on receptors containing GluN1-4b (Asn70Cys) and GluN2B (Thr324Cys). In contrast, a 2.5-fold potentiation was observed on breakage of the disulphide bond at the R1–R2 interface between GluN1-4b (Leu341Cys) and GluN2B (Asp210Cys) (Fig. 4c and Supplementary Fig. 11). This implies that locking the closed conformation in the GluN2B ATD bi-lobed structure by the R1–R2 crosslink results in downregulation of ion-channel activity. We next tested the effects of the disulphide bonds on sensitivity to ifenprodil. Although the R1–R1 crosslink had only a minor effect, the R1–R2 crosslink almost completely abolished inhibition by ifenprodil, even at 3 μM (Fig. 4d). When this R1–R2 disulphide crosslink was broken by the application of DTT, the mutant receptors regained sensitivity to ifenprodil, to a similar extent to that of receptors composed of wild-type GluN1-4b and GluN2B (Asp210Cys) in non-reducing conditions (Fig. 4d and Supplementary Fig. 12). This indicates that ifenprodil cannot bind to the GluN1b–GluN2B ATD when the R1–R2 interaction is locked and thus, when the GluN2B ATD clamshell is closed. Taken together, the experiments described above indicate that the binding of ifenprodil requires an opening of the GluN2B bi-lobed structure and that inhibition by ifenprodil involves closure of the clamshell through the GluN1b R1–GluN2B R2 interaction (Fig. 4e).

This study shows that phenylethanolamine binds at the GluN1–GluN2B subunit interface through an induced-fit mechanism and that allosteric inhibition involves stabilization of the GluN2B ATD clamshell structure in a closed conformation. The binding mechanism presented here provides a molecular blueprint for improving the design of therapeutic compounds targeting the ATD of the NMDA receptor.

METHODS SUMMARY

GluN1b and GluN2B ATDs were expressed as secreted proteins using the insect-cell/baculovirus system and purified using metal-chelate chromatography and size-exclusion chromatography. Crystallization was performed in hanging-drop vapour diffusion configuration in a buffer containing 20% PEG3350, 150 mM KNO_3 and 50 mM HEPES-NaOH (pH 7.0) for the GluN1b ATD, or 3.0–3.5 M sodium formate and 0.1 M HEPES-NaOH (pH 7.5) for the GluN1b–GluN2B ATD heterodimer. Diffraction data sets obtained at 100 K were indexed, integrated and scaled using HKL2000. The GluN1b ATD structure was solved by the single anomalous diffraction phasing method using Se-Met-incorporated crystals, and the GluN1b–GluN2B ATD structures were solved by molecular replacement using coordinates of GluN1b ATD and GluN2B ATD (Protein Data Bank code 3JPW[10]). Model refinement was conducted using the program Phenix[21]. Experiments involving analytical ultracentrifugation and isothermal titration calorimetry were conducted using the purified protein samples in their glycosylated form. Ion-channel activities of full-length NMDA receptors were measured by whole-cell recording

from cRNA-injected *Xenopus laevis* oocytes, using a two-electrode voltage-clamp configuration.

Full Methods and any associated references are available in the online version of the paper at www.nature.com/nature.

Received 20 January; accepted 6 May 2011.
Published online 15 June 2011.

1. Gotti, B. *et al.* Ifenprodil and SL 82.0715 as cerebral anti-ischemic agents. I. Evidence for efficacy in models of focal cerebral ischemia. *J. Pharmacol. Exp. Ther.* **247,** 1211–1221 (1988).
2. Koller, M. & Urwyler, S. Novel *N*-methyl-D-aspartate receptor antagonists: a review of compounds patented since 2006. *Expert Opin. Ther. Pat.* **20,** 1683–1702 (2010).
3. Hansen, K. B., Furukawa, H. & Traynelis, S. F. Control of assembly and function of glutamate receptors by the amino-terminal domain. *Mol. Pharmacol.* **78,** 535–549 (2010).
4. Mony, L., Kew, J. N., Gunthorpe, M. J. & Paoletti, P. Allosteric modulators of NR2B-containing NMDA receptors: molecular mechanisms and therapeutic potential. *Br. J. Pharmacol.* **157,** 1301–1317 (2009).
5. Traynelis, S. F. *et al.* Glutamate receptor ion channels: structure, regulation, and function. *Pharmacol. Rev.* **62,** 405–496 (2010).
6. Gallagher, M. J., Huang, H., Pritchett, D. B. & Lynch, D. R. Interactions between ifenprodil and the NR2B subunit of the *N*-methyl-D-aspartate receptor. *J. Biol. Chem.* **271,** 9603–9611 (1996).
7. Williams, K. Ifenprodil discriminates subtypes of the *N*-methyl-D-aspartate receptor: selectivity and mechanisms at recombinant heteromeric receptors. *Mol. Pharmacol.* **44,** 851–859 (1993).
8. Ewald, R. C. & Cline, H. T. Cloning and phylogenetic analysis of NMDA receptor subunits NR1, NR2A and NR2B in *Xenopus laevis* tadpoles. *Front. Mol. Neurosci.* **2,** 4 (2009).
9. Schmidt, C. & Hollmann, M. Molecular and functional characterization of *Xenopus laevis N*-methyl-D-aspartate receptors. *Mol. Cell. Neurosci.* **42,** 116–127 (2009).
10. Karakas, E., Simorowski, N. & Furukawa, H. Structure of the zinc-bound amino-terminal domain of the NMDA receptor NR2B subunit. *EMBO J.* **28,** 3910–3920 (2009).
11. Kumar, J., Schuck, P., Jin, R. & Mayer, M. L. The N-terminal domain of GluR6-subtype glutamate receptor ion channels. *Nature Struct. Mol. Biol.* **16,** 631–638 (2009).
12. Jin, R. *et al.* Crystal structure and association behaviour of the GluR2 amino-terminal domain. *EMBO J.* **28,** 1812–1823 (2009).
13. Clayton, A. *et al.* Crystal structure of the GluR2 amino-terminal domain provides insights into the architecture and assembly of ionotropic glutamate receptors. *J. Mol. Biol.* **392,** 1125–1132 (2009).
14. Sobolevsky, A. I., Rosconi, M. P. & Gouaux, E. X-ray structure, symmetry and mechanism of an AMPA-subtype glutamate receptor. *Nature* **462,** 745–756 (2009).
15. Gielen, M., Siegler Retchless, B., Mony, L., Johnson, J. W. & Paoletti, P. Mechanism of differential control of NMDA receptor activity by NR2 subunits. *Nature* **459,** 703–707 (2009).
16. Rachline, J., Perin-Dureau, F., Le Goff, A., Neyton, J. & Paoletti, P. The micromolar zinc-binding domain on the NMDA receptor subunit NR2B. *J. Neurosci.* **25,** 308–317 (2005).
17. Malherbe, P. *et al.* Identification of critical residues in the amino terminal domain of the human NR2B subunit involved in the RO 25-6981 binding pocket. *J. Pharmacol. Exp. Ther.* **307,** 897–905 (2003).
18. Masuko, T. *et al.* A regulatory domain (R1–R2) in the amino terminus of the *N*-methyl-D-aspartate receptor: effects of spermine, protons, and ifenprodil, and structural similarity to bacterial leucine/isoleucine/valine binding protein. *Mol. Pharmacol.* **55,** 957–969 (1999).
19. Perin-Dureau, F., Rachline, J., Neyton, J. & Paoletti, P. Mapping the binding site of the neuroprotectant ifenprodil on NMDA receptors. *J. Neurosci.* **22,** 5955–5965 (2002).
20. Lee, C. H. & Gouaux, E. Amino terminal domains of the NMDA receptor are organized as local heterodimers. *PLoS ONE* **6,** e19181 (2011).
21. Adams, P. D. *et al.* PHENIX: building new software for automated crystallographic structure determination. *Acta Crystallogr. D* **58,** 1948–1954 (2002).

Supplementary Information is linked to the online version of the paper at www.nature.com/nature.

Acknowledgements We thank the staff at X25 and X29 at the National Synchrotron Light Source for beamline support. M. Mayer is thanked for comments on this work. We also thank D. Raleigh for the use of analytical ultracentrifugation. GluN1 clones from *Xenopus laevis* were gifts from M. Hollmann and H. Cline. This work was supported by NIH MH085926, the Alzheimer's Association and a donation from the Fox family (to H.F.). H.F. was also funded by a scientist development grant from the American Heart Association. E.K. is supported by a NARSAD Lieber Young Investigator Award.

Author Contributions The project was initiated by E.K. and H.F. All of the experiments were designed by E.K. and H.F. Crystallographic studies, isothermal calorimetry and analytical ultracentrifugation were carried out by E.K. Electrophysiology and crosslinking experiments were conducted by H.F. Technical support was given by N.S. The manuscript was written by H.F. and E.K.

Author Information Structural coordinates are deposited in the Protein Data Bank with accession codes 3QEK for GluN1b ATD, 3QEL for GluN1b–GluN2B ATD in complex with ifenprodil and 3QEM for GluN1b–GluN2B ATD in complex with Ro 25-6981. Reprints and permissions information is available at www.nature.com/reprints. The authors declare no competing financial interests. Readers are welcome to comment on the online version of this article at www.nature.com/nature. Correspondence and requests for materials should be addressed to H.F. (furukawa@cshl.edu).

METHODS

Expression, purification and crystallization of GluN1b and GluN2B ATDs. The *Xenopus laevis* GluN1b ATD (Met 1 to Glu 408), containing Cys22Ser, Asn61Gln and Asn371Gln mutations, was C-terminally fused to a thrombin cleavage site followed by an octa-histidine tag. The *Xenopus laevis* GluN1b ATD and rat GluN2B ATD[10] constructs were individually expressed or co-expressed using the High Five (*Trichoplusia ni*) baculovirus system (DH10multibac)[22]. Purification was performed using a similar method to that described previously[10] except that the proteins were de-glycosylated by endoglycosidase F1 after purification by metal-chelate chromatography, and 1 μM ifenprodil or 1 μM Ro 25-6981 was included in the running buffer of size-exclusion chromatography (Superdex200) for isolation of the GluN1b–GluN2B ATD complex. The proteins used for isothermal titration calorimetry and sedimentation experiments were purified without the endoF1 de-glycosylation step and in the absence of ifenprodil or Ro 25-6981. Se-Met-incorporated GluN1b ATD proteins were expressed using methionine-free media (ESF921) supplemented with DL-Se-Met (Sigma) at 100 mg l^{-1} (ref. 10). The GluN1b ATD and GluN1b–GluN2B ATDs were crystallized by hanging-drop vapour diffusion at 17 °C by mixing the protein (8 mg ml^{-1}) at a 1:1 ratio with a reservoir solution containing 20% PEG3350, 150 mM KNO_3 and 50 mM HEPES-NaOH (pH 7.0) for GluN1b ATD, or at a 2:1 ratio with a solution containing 3.0–3.5 M sodium formate and 0.1 M HEPES (pH 7.5) for the GluN1b/GluN2B ATDs.

Data collection and structural analysis. Crystals were cryoprotected in buffers containing 20% PEG3350, 150 mM KNO_3, 50 mM HEPES-NaOH (pH 7.0) and 20% glycerol for GluN1b ATD, or 5 M sodium formate and 0.1 M HEPES-NaOH (pH 7.5) for GluN1b–GluN2B ATDs. X-ray diffraction data were collected at the X25 and X29 beamlines at the National Synchrotron Light Source and processed using HKL2000 (ref. 23). Single anomalous diffraction data for the Se-Met-incorporated GluN1b ATD crystals were collected at the peak wavelength (0.9788 Å) and used for phasing by the program SHARP[24]. The initial model was built using flex-wArp[25]. The crystal structure of GluN1b–GluN2B ATD was solved by molecular replacement using the coordinates of GluN1b ATD and GluN2B ATD[10] (PDB code: 3JPW) with the program PHASER[26]. The models were built using COOT[27] and structural refinement was performed using the program PHENIX[21].

Isothermal titration calorimetry. Proteins were dialysed overnight before the experiment against a buffer containing 150 mM NaCl, 20 mM Tris-HCl (pH 7.4) and 10% glycerol. Isothermal titration calorimetry measurements were performed using VP-ITC (MicroCal) by successive injections at 27 °C of 5 μl of 0.15 mM ifenprodil to 0.01 mM GluN1b ATD, 10 μl of 0.25 mM ifenprodil to 0.007 mM GluN2B ATD, 5 μl of 0.15 mM ifenprodil to 0.01 mM GluN1b–GluN2B ATD complex and 5 μl of 0.05 mM Ro 25-6981 to 0.007 mM GluN1b–GluN2B ATD complex. Data analysis was done using the software Origin 7.0 (Origin Labs).

Analytical ultracentrifugation. Sedimentation velocity and equilibrium experiments were performed using a Beckman Coulter Optima XL-I analytical ultracentrifuge. Proteins were dialysed against a buffer containing 150 mM NaCl and 20 mM Tris (pH 7.4), with or without 10 μM ifenprodil. Sedimentation velocity experiments were performed by centrifuging protein samples loaded on 2-sector centrepieces at 42,000 r.p.m. at 20 °C. Concentration gradients were measured using interference optics or absorbance optics at a wavelength of 280 nm or 230 nm depending on the protein concentrations loaded (0.01, 0.05, 0.1, 0.5 and 1.2 mg ml^{-1} for GluN1b–GluN2B ATD in the presence and absence of ifenprodil; 0.1 and 1.2 mg ml^{-1} for GluN1b ATD and 0.1, 0.5 and 5 mg ml^{-1} for GluN2B ATD). Data were analysed using the continuous c(s) and c(M) distribution models implemented in Sedfit[28]. The weighted-average sedimentation coefficient (S_w) was determined from the peak integration of c(s).

Sedimentation equilibrium experiments were performed using a 6-channel centrepiece loaded with 100-μl protein samples at protein concentrations of 0.05, 0.1 and 0.3 mg ml^{-1} in the presence or absence of 10 μM ifenprodil. The samples were centrifuged sequentially at 9,000, 13,000 and 18,000 r.p.m. and allowed to reach equilibrium at each speed. Absorbance measurements were performed at wavelengths 230, 250 and 280 nm to obtain measurements at low and high protein concentrations. Global analysis of the data for multiple protein concentrations and rotor speeds was performed using single-species and $A + B \leftrightarrow AB$ models implemented in Heteroanalysis v1.1.44 (University of Connecticut).

Electrophysiology. Recombinant GluN1/GluN2B NMDA receptors were expressed by co-injecting 0.1–0.5 ng of wild-type or mutant rat GluN1 and GluN2B cRNAs into defolliculated *Xenopus laevis* oocytes. The two-electrode voltage-clamp recordings were performed using agarose-tipped microelectrodes (0.4–1.0 MΩ) filled with 3 M KCl at a holding potential of −40 mV. The bath solution contained 5 mM HEPES, 100 mM NaCl, 0.3 mM $BaCl_2$ and 10 mM Tricine at pH 7.4 (adjusted with KOH). Currents were evoked by the application of glycine and L-glutamate at 100 μM each. Inhibition by ifenprodil was monitored in the presence of agonists and various concentrations of ifenprodil. For redox experiments, the oocytes were preincubated in the bath solution supplemented with 2 mM DTT for 3 min before recording in the continuous presence of 2 mM DTT. Data were acquired and analysed by the program Pulse (HEKA).

Cysteine crosslinking and western blot. Single point mutations were incorporated into the genes encoding full-length rat GluN1-4b and GluN2B in the pCI vector (Promega). Human embryonic kidney 293 cells were transfected by Fugene HD (Roche) with a mixture of 0.5 μg of the GluN1-4b plasmid and 1 μg of the GluN2B plasmid. Cells were harvested 24–48 h after transfection and resuspended in a buffer containing 20 mM Tris-HCl (pH 7.4), 150 mM NaCl, 1% dodecyl-maltoside and a protease-inhibitor cocktail (Roche), as previously described[29]. After centrifugation at 150,000*g*, the supernatant was subjected to SDS–polyacrylamide gel electrophoresis (4–15%) in the presence or absence of 100 mM DTT. The proteins were transferred to Hybond-ECL nitrocellulose membranes (GE Healthcare). The membranes were blocked with TBST (20 mM Tris-HCl (pH 7.4), 150 mM NaCl and 0.1% Tween-20) containing 10% milk, then incubated with mouse monoclonal antibodies against GluN1 (MAB 1586, Millipore) or GluN2B (Invitrogen), followed by HRP-conjugated anti-mouse antibodies (GE Healthcare). Protein bands were detected by ECL detection kit (GE Healthcare).

22. Fitzgerald, D. J. *et al.* Protein complex expression by using multigene baculoviral vectors. *Nature Methods* **3,** 1021–1032 (2006).
23. Otwinowski, Z. & Minor, W. Processing of X-ray diffraction data collected in oscillation mode. *Methods Enzymol.* **276,** 307–326 (1997).
24. de La Fortelle, E. & Bricogne, G. Maximum-likelihood heavy-atom parameter refinement for multiple isomorphous replacement and multiwavelength anomalous diffraction methods. *Methods Enzymol.* **276,** 472–494 (1997).
25. Cohen, S. X. *et al.* Towards complete validated models in the next generation of ARP/wARP. *Acta Crystallogr. D* **60,** 2222–2229 (2004).
26. McCoy, A. J. *et al.* Phaser crystallographic software. *J. Appl. Cryst.* **40,** 658–674 (2007).
27. Emsley, P. & Cowtan, K. Coot: model-building tools for molecular graphics. *Acta Crystallogr. D* **60,** 2126–2132 (2004).
28. Schuck, P. Size-distribution analysis of macromolecules by sedimentation velocity ultracentrifugation and Lamm equation modeling. *Biophys. J.* **78,** 1606–1619 (2000).
29. Furukawa, H., Singh, S. K., Mancusso, R. & Gouaux, E. Subunit arrangement and function in NMDA receptors. *Nature* **438,** 185–192 (2005).